CSIRO PUBLISHING

Australian Journal of Physics

Volume 52, 1999

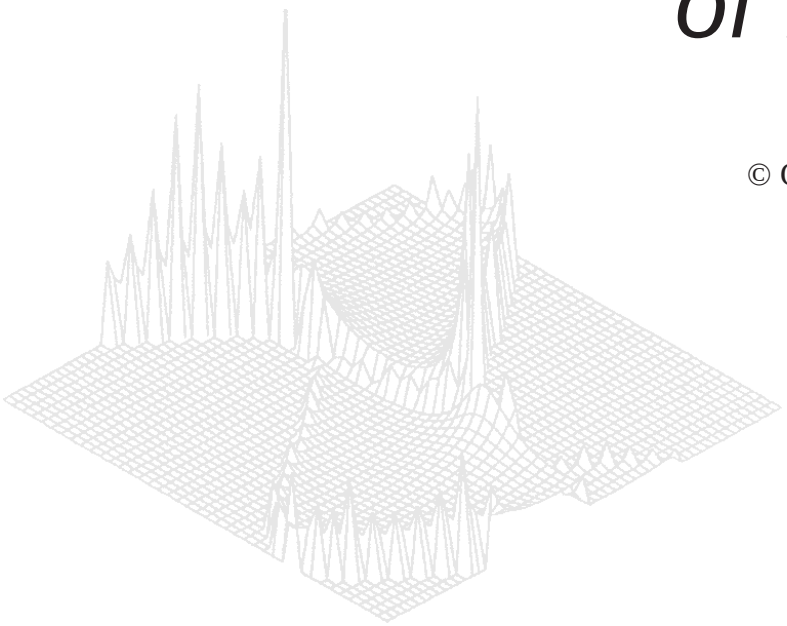

A journal for the publication of
original research in all branches of physics

www.publish.csiro.au/journals/ajp

All enquiries and manuscripts should be directed to
Australian Journal of Physics
CSIRO PUBLISHING
PO Box 1139 (150 Oxford St)
Collingwood Telephone: 61 3 9662 7626
Vic. 3066 Facsimile: 61 3 9662 7611
Australia Email: peter.robertson@publish.csiro.au

Published by **CSIRO** PUBLISHING
for CSIRO Australia and
the Australian Academy of Science

Aust. J. Phys., 1999, **52**, 397–420

Recent Developments of Resonant Auger Transitions: Predictions and Propensity Rules for the Dynamic Spin Polarisation*

B. Lohmann

Westfälische Wilhelms-Universität Münster,
Institut für Theoretische Physik I,
Wilhelm-Klemm-Str. 9, D-48149 Münster, Germany.

Abstract

The angular distribution and spin polarisation of the resonantly photoexcited $Xe^*(4d_{5/2}^{-1}\,6p_{3/2})$ $N_5O_{2,3}O_{2,3}$ Auger spectrum is investigated. The two-step model has been used which allows us to independently determine the dynamic parameters of the primary excitation and the Auger emission process. Assuming either a fully circularly or linearly polarised photon beam the dynamic parameters determining the primary photoexcitation become constant numbers independent of the matrix elements. Applying a relativistic distorted wave approximation the relevant numbers describing the Auger decay dynamics, i.e. relative intensities, angular distribution and spin polarisation parameters have been calculated, and are compared with experimental and other theoretical data. With this, predictions for the spin polarisation vector are possible. A large degree of dynamic spin polarisation has been found for all Auger transitions to a final state with $J_f = \frac{1}{2}$. This is in contrast to earlier calculations for diagram Auger transitions. Recently, we have given an explanation for this deriving propensity rules for resonant Auger transitions. The propensity rules allow for predictions for which Auger line a large dynamic spin polarisation can be expected. The predictions are in accord with our multiconfigurational Dirac–Fock calculations for the resonant Xe $N_5O_{2,3}O_{2,3}$ and Ar $L_3M_{2,3}M_{2,3}$ Auger multiplets. It is demonstrated that the effect of a large spin polarisation is caused by a large shift of the scattering phase of the emitted $\varepsilon s_{1/2}$ partial waves, whereas a small spin polarisation is due to a cancellation between the Coulomb and scattering phases of the partial waves.

1. Introduction

The observation of the angular distribution and spin polarisation of Auger electrons has been recognised as a useful tool to obtain more refined information about the Auger emission process. As has been pointed out for example by Kessler (1985), such experiments can be seen as a step further towards a so-called *complete experiment*.

While the Auger spectrum has been investigated theoretically and experimentally by many groups—a good overview may be found in the review by Schmidt (1992)—and several investigations focused on the angle resolved spectrum (see Schmidt 1992 and more recently e.g. Lohmann and Fritzsche 1996), the number

* Refereed paper based on a contribution to the Australia–Germany Workshop on Electron Correlations held in Fremantle, Western Australia, on 1–6 October 1998.

 10.1071/PH99019 0004-9506/99/030397$10.00

of investigations concerning the spin polarisation of Auger electrons is still small (e.g. Klar 1980; Hahn *et al.* 1985; Kabchnik *et al.* 1988; Merz and Semke 1990; Kuntze *et al.* 1993; Lohmann *et al.* 1993; Müller *et al.* 1995; Lohmann 1996). Expanding the spin polarisation vector in terms of its cartesian components, the process of generating a non-zero spin polarisation of the emitted Auger electrons is different for the in-reaction plane components and the components perpendicular to the reaction plane, respectively.

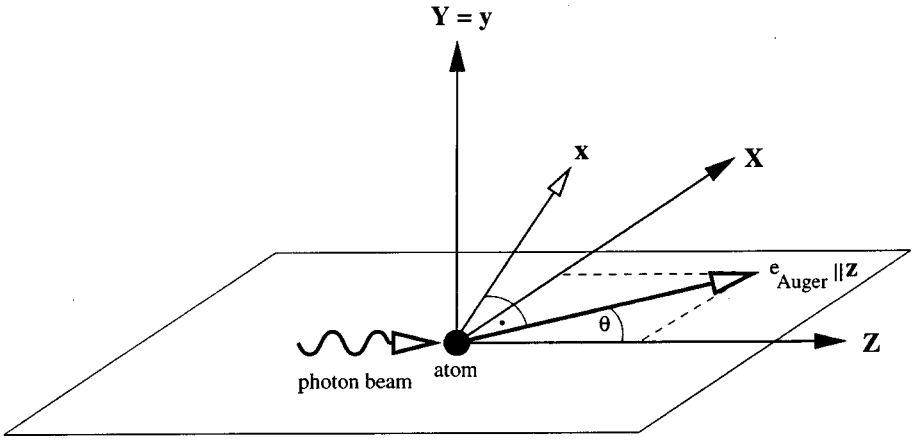

Fig. 1. Coordinate frame and reaction plane. The reaction plane is spanned by the incoming synchrotron beam axis $\mathbf{k}_\gamma$ and the direction of Auger emission $\mathbf{k}_a$.

Restricting ourselves to the case of photoionisation/excitation, the components of the spin polarisation vector of Auger emission in the reaction plane (see Fig. 1), defined by the incoming synchrotron beam axis and the direction of Auger emission, can be only observed if the incoming synchrotron beam is circularly polarised and are therefore denoted as *intrinsic*. From a physical point of view this is due to the fact that a non-zero spin polarisation of the emitted Auger electrons can be only generated via *polarisation transfer*. This has been investigated e.g. by Kuntze *et al.* (1993), Lohmann *et al.* (1993), Müller *et al.* (1995) and Lohmann (1996).

The component of the spin polarisation vector perpendicular to the reaction plane is usually denoted as *dynamic spin polarisation*. This case is physically interesting. Here, the spin polarisation of the Auger electrons is generated via dynamic effects during the Auger emission. As has been pointed out by Klar (1980), its observation should be possible even if the target and the photon beam are unpolarised. The first experiment by Hahn *et al.* (1985), using electron impact ionisation, reported an almost vanishing dynamic spin polarisation for the so-called diagram or normal Auger transitions. This has also been confirmed by theoretical calculations (Kabachnik *et al.* 1988; Lohmann *et al.* 1993). Recently, experiments have been done to measure the dynamic spin polarisation for so-called resonantly excited Auger transitions, and a large dynamic spin polarisation has been found for certain Auger lines (Snell *et al.* 1996*a*, 1996*b*).

The aim of this work is to review the theory and to provide further theoretical data to compare with other theories and experiments. In addition, we give predictions for the spin polarisation vector and, by applying our recently derived propensity rules (Lohmann 1998*a*), give predictions whether a large dynamic spin polarisation can be expected for certain lines of the resonantly excited Auger spectrum, or not. This is actually the first time that, with respect to Auger transitions, theory has been able to fulfill a basic request of experimentalists (Kessler and Merz 1984): to predict whether measurable numbers can be expected from an angle and spin resolved Auger emission experiment. Due to the feasibility of such experiments, the need for a synchrotron line, Mott chamber, etc. there has been an urgent need for such guidelines.

In the next section an outline of the theoretical background will be given. By applying a two-step model the general equations for angular distribution and spin polarisation of Auger emission after photoexcitation will be discussed. The dynamics of the primary photoexcitation and the subsequent Auger emission are discussed in more detail for different polarisation states of the incoming synchrotron beam. A brief outline of the calculational model will be given. In Section 3 our results for the resonant Xe $N_5O_{2,3}O_{2,3}$ Auger transitions will be given and discussed. The relevant numbers of relative intensities, angular distribution and spin polarisation parameters will be compared with other theoretical and experimental data in Section 4. We will consider the dynamic spin polarisation in more detail. Particular attention will be given to the question of large versus small dynamic spin polarisation, i.e. under which conditions a large dynamic spin polarisation can be expected. We will derive and discuss the propensity rules which allow for the first time predictions for a large dynamic spin polarisation in resonant Auger transitions. Our numerical results of a large dynamic spin polarisation for an unresolved final state will be compared to recent experimental data. Predictions for the spin polarisation vector will be given for certain Auger lines. Some concluding remarks will be given in the last section.

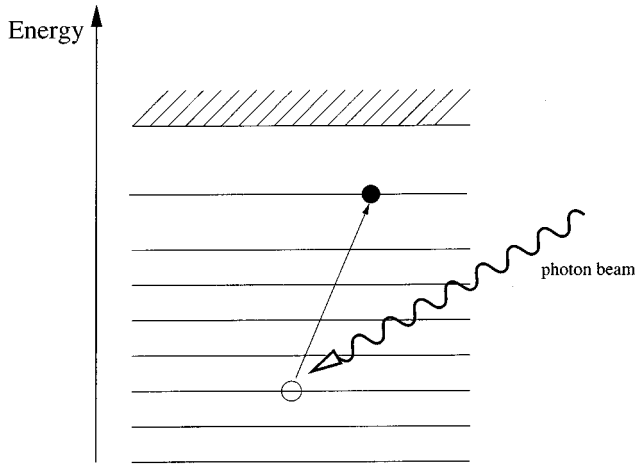

Fig. 2. The primary photoexcitation.

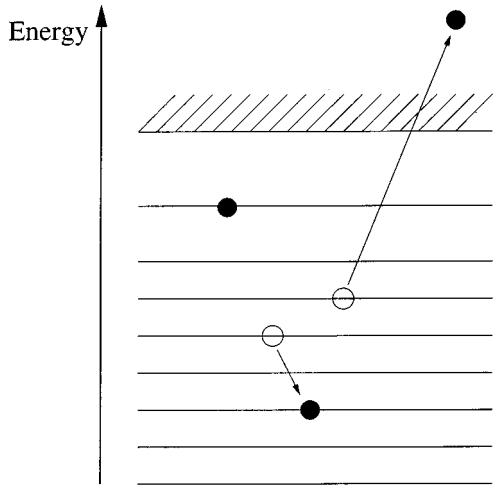

Fig. 3. The resonant Auger emission process.

2. Theory

(2a) General Considerations

The present understanding of the Auger emission is that of a two-step process (e.g. see the review by Mehlhorn 1990). What is commonly known as Auger transitions are the so-called *diagram* transitions, i.e. the target atom is, in a first step, ionised in an inner electronic shell and decays subsequently via Auger emission leaving behind a doubly ionised atom. In this paper we consider the *resonant* Auger emission in more detail. Considering a primary photoexcitation process the resonant Auger process can be written as

$$\gamma + A \longrightarrow A^* \tag{1}$$

$$\searrow\ A^* \longrightarrow A^{+*} + e_{\mathrm{Auger}}\,. \tag{2}$$

In a first step, which is shown in Fig. 2, an inner shell electron is excited via photoabsorption into a Rydberg level. After a certain lifetime, the excited atom decays via Auger emission while the excited electron remains in its Rydberg level leaving the target atom in a singly ionised excited state. The resonant Auger emission is illustrated in Fig. 3.

(2b) Angular Distribution and Spin Polarisation of Resonant Auger Electrons

The general equations of angular distribution and spin polarisation of Auger electrons have been recently derived by Kleiman *et al.* (1999) assuming a primary photoionisation. Adopting their results the expressions for angular distribution and spin polarisation of a resonant Auger emission after primary photoexcitation can be derived. The general expression for the angular distribution may be written as

$$I(\theta) = \frac{I_0}{4\pi}\left(1 + \alpha_2\left[\mathcal{A}_{20}\,P_2(\cos\theta) + \sqrt{\tfrac{3}{2}}\,\mathrm{Re}\mathcal{A}_{22}\,\sin^2\theta\right]\right)\,, \tag{3}$$

where I_0 denotes the total intensity integrated over the solid angle. Since we are applying a two-step model the angular distribution parameters can be factorised into two terms. The parameters $\mathcal{A}_{KQ}$ contain information about the dynamics of the primary excitation process. They are related to the state multipoles of Blum (1996) and are basically a function of the beam energy and of the polarisation states of the incoming beam and the target. In the following, we assume the target atom to be unpolarised. For a primary photoexcitation the dipole approximation can be applied. This yields a general restriction for the state multipoles and, thus, only excitation parameters $\mathcal{A}_{KQ}$ with rank $K \leq 2$ can contribute to the general expressions for angular distribution and spin polarisation. In particular, the second rank tensor parameter $\mathcal{A}_{20}$ and the first rank tensor $\mathcal{A}_{10}$ are known as alignment and orientation parameters, respectively.

The angular distribution parameter α_2 contains information solely about the Auger decay dynamics. It is basically a function of Auger transition amplitudes and scattering phases. Explicit expressions may be found e.g. in Lohmann and Fritsche (1994).

Observing the angle resolved intensity at an angle $\theta \neq 0°$ defines a reaction plane. The related coordinate frame is illustrated in Fig. 1. Then, the cartesian components of the spin polarisation vector, with respect to the helicity system of the emitted Auger electrons, i.e. z-axis $\parallel \mathbf{k}_a$, can be written as

$$p_x(\theta) = \frac{(\xi_1\,\mathcal{A}_{10} + \sqrt{6}\,\xi_2\,\mathrm{Im}\mathcal{A}_{22})\sin\theta}{1 + \alpha_2(\mathcal{A}_{20}\,P_2(\cos\theta) + \sqrt{\tfrac{3}{2}}\,\mathrm{Re}\mathcal{A}_{22}\,\sin^2\theta)}\,, \tag{4}$$

$$p_y(\theta) = \frac{-\tfrac{3}{2}\,\xi_2(\mathcal{A}_{20} - \sqrt{\tfrac{2}{3}}\,\mathrm{Re}\mathcal{A}_{22})\sin 2\theta}{1 + \alpha_2(\mathcal{A}_{20}\,P_2(\cos\theta) + \sqrt{\tfrac{3}{2}}\,\mathrm{Re}\mathcal{A}_{22}\,\sin^2\theta)}\,, \tag{5}$$

$$p_z(\theta) = \frac{\delta_1\,\mathcal{A}_{10}\,\cos\theta}{1 + \alpha_2(\mathcal{A}_{20}\,P_2(\cos\theta) + \sqrt{\tfrac{3}{2}}\,\mathrm{Re}\mathcal{A}_{22}\,\sin^2\theta)}\,. \tag{6}$$

As for the angular distribution, the spin polarisation parameters factorise into two terms. The photoexcitation dynamics is again described by the tensor parameters $\mathcal{A}_{KQ}$. In addition to the alignment parameter $\mathcal{A}_{20}$, the in-reaction plane components $p_x(\theta)$ and $p_z(\theta)$ also depend on the orientation parameter $\mathcal{A}_{10}$. All components depend on the real and imaginary parts of the additional alignment parameter $\mathcal{A}_{22}$. Both are related to certain polarisation states of the incoming synchrotron beam which will be discussed later. In addition, the $p_x(\theta)$ component of the spin polarisation vector also depends on the imaginary part of the excitation parameter $\mathcal{A}_{22}$.

Further information on the Auger decay dynamics can be obtained from the spin polarisation parameters δ_1, ξ_1 and ξ_2. Expressions for them may be found in e.g. Lohmann *et al.* (1993) or Kleiman *et al.* (1999). In particular, the

δ_1 and ξ_1 are related to the in-plane components of the spin polarisation vector. They can be observed only if the incoming synchrotron beam is circularly polarisation and are therefore denoted as intrinsic. The spin polarisation parameter ξ_2 is basically related to the component $p_y(\theta)$ of the spin polarisation vector perpendicular to the reaction plane. In principle, its observation should be possible even if the target and the photon beam are unpolarised, and ξ_2 is therefore denoted as a dynamic spin polarisation parameter, i.e. it can only be observed if the alignment of the intermediate excited state is dynamically transferred into a spin polarisation of the emitted Auger electron. As has been shown by Blum *et al.* (1986), this can only happen if explicit spin dependent forces are present during the Auger emission.

From their structure, the equations of angular distribution and spin polarisation of Auger emission are similar to relations obtained for the emission of photoelectrons.

(2c) Special Cases

Let us consider some special cases in more detail. For this, we first discuss the primary excitation process with respect to different polarisation states of the incoming synchrotron beam. Then, we consider the Auger emission in order to see how the general equations of angular distribution and spin polarisation are reduced for these cases.

Photoexcitation. For a primary photoexcitation process

$$\gamma + A \longrightarrow A^* \tag{7}$$

the neutral initial atomic state is excited via photoabsorption. The photoexcitation is illustrated in Fig. 2. The intermediate excited atomic state A^* is fully described by the set of tensor parameters

$$\mathcal{A}_{KQ} = \frac{\langle T(J)^+_{KQ} \rangle}{\langle T(J)^+_{00} \rangle} \,, \tag{8}$$

and, as has been pointed out in Section 2*b*, the dynamics of the photoexcitation is contained in the state multipoles $\langle T(J)^+_{KQ} \rangle$. The state multipoles describing the intermediate excited atomic ensemble can be related to the state multipoles $\langle \mathcal{T}^+_{\Gamma\gamma} \rangle$ of the incoming photon beam by (Lohmann 1998*b*)

$$\langle T(J)^+_{KQ} \rangle = B_{ex}(K) \, \langle \mathcal{T}^+_{\Gamma\gamma} \rangle \, \delta_{K,\Gamma} \, \delta_{Q,\gamma} \,, \tag{9}$$

where $B_{ex}(K)$ denotes the anisotropy parameter of photoexcitation, Γ and γ are rank and magnetic component of the photonic state multipoles and δ_{ij} denotes a Kronecker symbol. This relation is similar to the one which has been obtained recently by Kleiman *et al.* (1999) for the case of photoionisation.

Applying the dipole approximation and using standard methods of angular momentum algebra the photoexcitation parameter may be eventually expressed as

$$B_{ex}(K) = \frac{1}{2J_0+1}\,(-1)^{1+J+J_0+K} \begin{Bmatrix} 1 & 1 & K \\ J & J & J_0 \end{Bmatrix} J||\hat{\mathbf{d}}||J_0|^2\,, \tag{10}$$

where $\hat{\mathbf{d}}$ denotes the dipole operator and J_0 and J denote the total angular momenta of the initial and intermediate excited state, respectively. From equation (10), it is evident that B_{ex} is a real quantity. In particular, considering an initial atomic state with total angular momentum $J_0 = 0$, i.e. the rare gases, the symmetry relations of the $6j$-symbols yield $J = 1$ and equation (10) can be further reduced to

$$B_{ex}^{J_0=0}(K) = B_{ex}^{J_0=0}(0) = \tfrac{1}{3}\,|1||\hat{\mathbf{d}}||0|^2\,. \tag{11}$$

Thus, the anisotropy parameters become constant numbers, independent of their rank K. This case is of importance for photoexcitation and subsequent Auger decay of the rare gases. The tensor parameters of photoexcitation are therefore directly proportional to the state multipoles describing the polarisation state of the incoming synchrotron beam.

Generally, circularly polarisation synchrotron radiation has a linearly polarisation admixture and vice versa. Therefore, besides the usual alignment and orientation parameters $\mathcal{A}_{20}$ and $\mathcal{A}_{10}$, additional tensors $\mathcal{A}_{KQ}$ with $Q \neq 0$ can occur. This is because the reduced density matrix cannot be diagonalised for arbitrarily polarisation synchrotron radiation. The specific occurrence of additional parameters depends however on an explicit choice of the quantisation axis. For the following we will choose the quantisation axis parallel to the incoming synchrotron beam axis, i.e. z-axis $\parallel \mathbf{k}_\gamma$.

Commonly, the polarisation of a photon beam is described in terms of Stokes parameters. They can be easily related to the associated state multipoles which are shown in Table 1. Note that, e.g. the parameter $\langle \mathcal{T}_{11}^{+} \rangle$, which is zero in our case can be non-zero if a different quantisation axis is chosen.

Considering a fully circularly polarisation photon beam, i.e. $\eta_2 = 1$, we obtain

$$\begin{aligned} \mathcal{A}_{10} &= \sqrt{\tfrac{3}{2}}, \qquad & \mathcal{A}_{20} &= \sqrt{\tfrac{1}{2}} \\ \text{and} \qquad & & \mathcal{A}_{22} &= 0\,. \end{aligned} \tag{12}$$

For this case only the two common tensor parameters of orientation and alignment are non-zero while the parameter $\mathcal{A}_{22}$ vanishes. From the discussion above, and applying the results of equations (9) and (11), it is evident that the expressions for orientation and alignment are fully analytic for photoexcitation from the ground state of the rare gases.

On the other hand, assuming a fully linearly polarisation photon beam, i.e. $\eta_3 = \pm 1$, we obtain

$$\begin{aligned} &\mathcal{A}_{10} = 0, \qquad && \mathcal{A}_{20} = \sqrt{\tfrac{1}{2}}, \\ &\mathrm{Im}\mathcal{A}_{22} = 0 \qquad && \text{and} \quad \mathrm{Re}\mathcal{A}_{22} = \mp\sqrt{\tfrac{3}{2}}\,. \end{aligned} \tag{13}$$

While the orientation parameter $\mathcal{A}_{10}$ vanishes in this case, the real part of the parameter $\mathcal{A}_{22}$ becomes non-zero.

Table 1. State multipoles of an arbitrarily polarisation photon beam and their connection to the Stokes parameters

The photon beam axis has been chosen as the quantisation axis. Multipoles of rank $K > 2$ must be zero due to dipole-selection rules. [From Lohmann (1998*b*).]

Stokes parameters		State multipoles
I	=	$\sqrt{3}\langle\mathcal{T}^+_{00}\rangle$
$I\eta_2$	=	$\sqrt{2}\langle\mathcal{T}^+_{10}\rangle$
0	=	$\langle\mathcal{T}^+_{1\pm1}\rangle$
I	=	$\sqrt{6}\langle\mathcal{T}^+_{20}\rangle$
0	=	$\langle\mathcal{T}^+_{2\pm1}\rangle$
$I\eta_3$	=	$-2\mathrm{Re}\langle\mathcal{T}^+_{22}\rangle$
$I\eta_1$	=	$2\mathrm{Im}\langle\mathcal{T}^+_{22}\rangle$

It is worth noting that the alignment parameter $\mathcal{A}_{20}$ is always different from zero, independent of the choice of quantisation axis and of the polarisation state of the incoming synchrotron beam. This is caused by the fact that photons are spin-one particles and are therefore, due to the transverse character of the electromagnetic field, always aligned. During photoexcitation, this alignment is eventually transferred to the excited target.

A physical interpretation of the parameter $\mathcal{A}_{20}$ has been given earlier by Hertel and Stoll (1977) who have shown that a non-zero alignment results in an anisotropic deformation of the electronic charge cloud into a *cigar-like* shape which is axially symmetric to the incoming photon beam axis. Using a linearly polarisation photon beam, and thus having a non-vanishing parameter $\mathcal{A}_{22}$, yields a further deformation of the ionic charge cloud, i.e. the cigar-like shape of the electronic charge cloud is further compressed with respect to one of its principal axes.

Eventually, we note an interesting relation between the alignment parameters $\mathcal{A}_{20}$ and $\mathcal{A}_{22}$ (Kleiman *et al.* 1999):

$$\mathcal{A}_{22} = \mathcal{A}_{20}\sqrt{\tfrac{3}{2}}\left(-\eta_3 + i\eta_1\right). \tag{14}$$

This result is of physical importance since it demonstrates the fact that, besides the intrinsic alignment $\mathcal{A}_{20}$, which is generally transferred from the unpolarisation photon beam to the intermediate ionic state, any additional alignment, generated from linearly polarisation photons, can always be directly related to the usual alignment $\mathcal{A}_{20}$.

Auger emission. After a certain lifetime the resonantly excited intermediate atomic state decays via Auger emission:

$$A^* \longrightarrow A^{+*} + e_{\mathrm{Auger}}\,, \tag{15}$$

leaving a singly ionised target behind.

The Auger decay dynamics are described by the relative intensities I_0, the angular distribution parameter α_2, and the spin polarisation parameters δ_1,

ξ_1 and ξ_2 where the first two are the intrinsic parameters related to polarisation transfer and the latter to the dynamic spin polarisation.

As has been discussed in the previous section the intermediate excited atomic state is described by different sets of tensor parameters $\mathcal{A}_{KQ}$ for different polarisation states of the incoming synchrotron beam. Considering some polarisation states in more detail and applying these results to the general equations (3)–(6), the expressions for angular distribution and spin polarisation can be reduced.

By considering the case of a fully circularly polarisation photon beam, i.e. $|\eta_2| = 1$, the angular distribution may be written as

$$I(\theta) = \frac{I_0}{4\pi}\left(1 + \frac{\alpha_2}{\sqrt{2}}\,P_2(\cos\theta)\right)\,, \tag{16}$$

and the cartesian components of the spin polarisation vector can be reduced to

$$p_x(\theta) = \frac{\sqrt{3}\,\xi_1 \sin\theta}{\sqrt{2} + \alpha_2\,P_2(\cos\theta)}\,, \tag{17}$$

$$p_y(\theta) = \frac{-\frac{3}{2}\,\xi_2 \sin 2\theta}{\sqrt{2} + \alpha_2\,P_2(\cos\theta)}\,, \tag{18}$$

$$p_z(\theta) = \frac{\sqrt{3}\,\delta_1 \cos\theta}{\sqrt{2} + \alpha_2\,P_2(\cos\theta)}\,. \tag{19}$$

Thus, besides the angular distribution, all components of the spin polarisation vector can be measured in this type of experiment. As a matter of fact, a circularly polarisation synchrotron beam has been used in a number of experiments focusing on the determination of the intrinsic spin polarisation parameters δ_1 and ξ_1 (e.g. Kuntze *et al.* 1993; Müller *et al.* 1995).

On the other hand, assuming a fully linearly polarisation photon beam with $\eta_3 = 1$ we get

$$I(\theta) = \frac{I_0}{4\pi}\left(1 + \frac{\alpha_2}{\sqrt{2}}\Big[2P_2(\cos\theta) - 1\Big]\right)\,, \tag{20}$$

$$p_x(\theta) = p_z(\theta) = 0\,, \tag{21}$$

$$p_y(\theta) = \frac{-3\,\xi_2 \sin 2\theta}{\sqrt{2} + \alpha_2\big(2P_2(\cos\theta) - 1\big)}\,. \tag{22}$$

This will be our major case of interest in the remainder of this work. Here, besides the angular distribution, only the component $p_y(\theta)$ of the spin polarisation vector perpendicular to the reaction plane can be experimentally observed. The two in-reaction plane components must be zero due to symmetry principles, i.e. a linear polarisation of the photon beam cannot create an in-reaction plane spin polarisation. However, as it ensures a maximum alignment the dynamic spin polarisation parameter can be best observed for this case. A typical experimental setup is to observe the dynamic spin polarisation at the *magic* angle, $\theta_m = 54{\cdot}74°$, i.e. the second Legendre polynomial vanishes, which yields

$$p_y(\theta_m) = \frac{\sqrt{8}\,\xi_2}{\alpha_2 - \sqrt{2}}\,. \tag{23}$$

As pointed out in the introduction p_y is found to be small even for most of the resonant Auger transitions, which is mainly caused by the fact that the α_2 parameter is commonly at least a magnitude larger than the dynamic spin polarisation parameter ξ_2. Thus, the spin polarisation is best observed as a function of ξ_2, only. We suggest observing the spin polarisation at the angle $\theta_\xi = 35{\cdot}26°$. For this angle the denominator becomes independent of α_2 and we obtain a simple relation between the spin polarisation vector component p_y and the dynamic spin polarisation parameter ξ_2, i.e.

$$p_y(\theta_\xi) = -2\,\xi_2\,. \tag{24}$$

Considering the opposite case, i.e. $\eta_3 = -1$, we obtain the, at a first glance, surprising result of an isotropic angular distribution and a vanishing spin polarisation:

$$I(\theta) = \frac{I_0}{4\pi}\left(1 + \frac{\alpha_2}{\sqrt{2}}\right)\,, \tag{25}$$

$$p_x(\theta) = p_y(\theta) = p_z(\theta) = 0\,. \tag{26}$$

This can however be explained as a direct outcome of the dipole approximation. Here, any information about the origin of the incident photons vanishes. Therefore, we only have to consider the direction of the electric field vector which oscillates perpendicular to the reaction plane. Thus, the system is invariant under reflection within all three planes, the $x-y$, the $y-z$ and the $x-z$ plane. Hence, all components of the spin polarisation vector vanish.

This effect is well-known for the case of photoionisation and has been widely used for the production of unpolarisation photoelectrons (Kleinpoppen 1997). However, with respect to Auger emission, this effect has not been experimentally demonstrated until today and, only recently, has been theoretically investigated in more detail (Kleiman *et al*. 1999).

Note that for the angular distribution this case is different to the integrated intensity over the solid angle. Here, we still have a dependence on the total intensity I_0 and the angular distribution parameter α_2.

(2d) Calculational Model

For obtaining the numerical data we employ a relativistic distorted wave approximation (RDWA). Here, the bound state wavefunctions of the excited intermediate and the ionised final state of the atom are constructed using the multiconfigurational Dirac–Fock (MCDF) computer code of Grant *et al.* (1980). Intermediate coupling has been taken into account. The mixing coefficients have been calculated with the MCDF code of Grant *et al.*, applying the average level calculation mode. The calculation of the Auger transition matrix elements is done applying a relaxed orbital method. Thus, the bound electron wavefunctions of the intermediate state are calculated in the field of the excited atom. On the other hand, the bound electron wavefunctions of the final state are calculated in the field of the singly ionised atom. Eventually, the continuum wavefunction of the Auger electron is evaluated by solving the Dirac equation with an intermediate coupling potential where electron exchange with the continuum has been taken into account. The intermediate coupling potential is constructed from the mixed configuration state functions (CSF) of the final ionic state. Thereby, we take into account that the ejected electron moves within the field of the residual ion. With this, the Auger transition matrix elements are obtained for calculating the anisotropy and spin polarisation parameters, respectively. Our present calculation exceeds the spectator model (see e.g. Kämmerling *et al.* 1990; Lohmann 1991; Hergenhahn *et al.* 1991), by fully taking into account the variation of the intermediate ionic charge cloud through the spectator electron. In particular, we carried out two types of calculations. In the first we neglect exchange, while our second calculation takes exchange interaction with the continuum into account.

3. Results: Resonant Xe $N_5O_{2,3}O_{2,3}$ Auger Transitions

We have calculated the transitions of the resonantly excited Xe $N_5O_{2,3}O_{2,3}$ Auger spectrum. In particular, we consider the resonant Auger transitions

$$\gamma + \mathrm{Xe}\,(^1\mathrm{S}_0) \longrightarrow \mathrm{Xe}^*\,(4\mathrm{d}_{5/2}^{-1}, 6\mathrm{p}_{3/2})_{J=1} \tag{27}$$

$$\searrow\ \mathrm{Xe}^{+*}(5\mathrm{p}_{1/2,3/2}^{-2}, 6\mathrm{p}_{3/2})_{J_f=1/2,\ldots,7/2} + e_{\mathrm{Auger}}\,. \tag{28}$$

As a rare gas, the Xe atoms have a closed shell structure. Thus, their ground state is a $^1\mathrm{S}_0$. Therefore, after a primary photoexcitation the intermediate excited state must have a total angular momentum $J = 1$ due to the dipole selection rules. Our main focus is the Auger lines which stem from an intermediate $4\mathrm{d}_{5/2}^{-1}$ inner shell hole. Thus, for a 4d → 6p excitation only the intermediate $(4\mathrm{d}_{5/2}^{-1}, 6\mathrm{p}_{3/2})_{J=1}$ state can be populated. Of course, a photoexcitation of the $(4\mathrm{d}_{3/2}^{-1}, 6\mathrm{p}_{1/2,3/2})_{J=1}$ states is possible, too. However, due to the fine structure splitting the $4\mathrm{d}_{5/2}^{-1}$ hole is well separated from the $4\mathrm{d}_{3/2}^{-1}$ fine structure state. The latter refers to the resonantly excited Xe $N_4O_{2,3}O_{2,3}$ Auger transitions instead.

The full set of parameters, i.e. relative intensities, angular anisotropy, and spin polarisation parameters has been calculated. Our data are shown in Table 2. We have only listed our numerical results where exchange has been taken into account. Our MCDF calculation includes for 13 CSF, i.e. all transitions according to equation (28). Since our calculation does not include the spin-flip transitions

which can, in principle, create a final $6p_{1/2}$ electron, we have not been able to calculate all lines of the spectrum. In Table 2, the Auger lines have been identified by their leading jj-coupled configuration state function. The resonantly excited Xe $N_5O_{2,3}O_{2,3}$ Auger spectrum has been also investigated by Aksela *et al.* (1995). As shown in Table 2, we adopt their notation of line numbers to identify the different final states for the remainder of this work.

Table 2. Energies, relative intensities, angular distribution and spin polarisation parameters for the $Xe^*(4d_{5/2}^{-1}6p_{3/2})$ $N_5O_{2,3}O_{2,3}$ Auger transitions

		Xe^* $(6p_{3/2})$ $N_5O_{2,3}O_{2,3}$					
Final states		Energy	Int.	Ang. & spin pol. par.			
(a)	(b)	(eV)	I_0†	α_2	δ_1	ξ_1	ξ_2
$\|([5\bar{p}^2 5p^2]_2 6p^1)5/2\rangle$	22	39·73	7·433	0·704	-0·143	-0·041	0·003
$([5\bar{p}^2 5p^2]_2 6p^1)7/2\rangle$	24	39·64	1·713	0·582	0·327	0·319	−0·041
$\|([5\bar{p}^2 5p^2]_2 6p^1)1/2\rangle$	23	39·54	1·403	−0·078	0·771	0·117	0·478
$\|([5\bar{p}^2 5p^2]_2 6p^1)3/2\rangle$	26	39·29	10·523	−0·726	-0·275	0·310	0·044
$\|([5\bar{p}^2 5p^2]_0 6p^1)3/2\rangle$	31	38·49	9·508	−0·654	0·060	0·626	0·004
$\|([5\bar{p}^1 5p^3]_1 6p^1)5/2\rangle$	32	38·47	0·189	0·214	0·833	0·710	0·007
$\|([5\bar{p}^1 5p^3]_1 6p^1)1/2\rangle$	36	38·37	6·984	−0·750	0·383	−0·751	−0·164
$\|([5\bar{p}^1 5p^3]_1 6p^1)3/2\rangle$	34	38·33	1·810	0·686	0·589	−0·049	−0·039
$\|([5\bar{p}^1 5p^3]_2 6p^1)7/2\rangle$	42	37·26	13·200	−0·109	0·348	0·719	−0·020
$\|([5\bar{p}^1 5p^3]_2 6p^1)3/2\rangle$	43	37·20	11·934	0·292	0·658	0·501	0·241
$\|([5\bar{p}^1 5p^3]_2 6p^1)1/2\rangle$	46	37·07	8·274	−0·291	0·648	0·509	−0·404
$\|([\bar{p}^1 5p^3]_2 6p^1)5/2\rangle$	44	37·01	6·052	0·668	1·041	0·206	0·053
$\|([5\bar{p}^0 5p^4]_0 6p^1)3/2\rangle$	67,68	34·52	20·977	−0·550	0·300	0·761	0·009

(a) The leading jj coupled configuration state function has been used to identify the state.
(b) Line numbers according to Aksela *et al.* (1995).
†The total intensity has been normalised to 100.

4. Comparison between Theory and Experiment

The resonantly excited Xe $N_5O_{2,3}O_{2,3}$ Auger spectrum has been investigated by several groups. In the following, we will therefore compare our results with other theories and experimental data.

(4a) Intensities

We carried out two calculations for the relative intensities of the resonantly excited Xe $N_5O_{2,3}O_{2,3}$ Auger spectrum. Our results are given in Table 3 together with other numerical and experimental data. Our calculation (b) neglects the exchange interaction while the next column, calculation (c), takes exchange with the continuum into account. In the next two columns, (d) and (e), the experimental data of Aksela *et al.* (1995) and Langer *et al.* (1996) are given. Columns (f) and (g) show the numerical data obtained by Aksela *et al.* and by Chen (1993) respectively.

Aksela *et al.* (1995) calculated the Xe $N_5O_{2,3}O_{2,3}$ Auger spectrum in a number of different approaches of which they identify their so-called *FE* calculation as best. (Further information may be found in the cited paper.) Thus, we only compare our data to this calculation.

Comparing our two calculations (b) and (c), the inclusion of exchange slightly decreases the intensity of the Auger transitions to the most bound final states, while transitions to states closer to threshold show a slight increase in intensity. For the Auger lines of the most bound states, i.e. transitions to the $(^3\mathrm{P})6\mathrm{p}\,^2\mathrm{D}_{5/2,7/2}$ and $^2\mathrm{S}_{1/2}$ final states (lines 22–24), there is good agreement between all theoretical calculations and the experimental data as well. However, for line no. 26, i.e. the Auger transition to the $(^3\mathrm{P})6\mathrm{p}\,^2\mathrm{P}_{3/2}$ final state, this behaviour changes. Though there is still good agreement between our calculations and that of Aksela *et al.* (1995), both calculations underestimate the experimental results (Aksela *et al.* 1995; Langer *et al.* 1996) by a factor of $\sim 1{\cdot}6$. The experimental data for this line are, however, well reproduced by the calculation of Chen (1993). The situation becomes worse for the Auger transition to the $(^1\mathrm{D})6\mathrm{p}\,^2\mathrm{F}_{7/2}$ final state, i.e. line no. 42. Here, our calculation including exchange is close to the calculation by Chen, while the calculation of Aksela *et al.* yields a result twice as large. Besides, none of the numerical calculations comes even close to the experimental results. While the numerical data overestimate the experiment by at least a factor of four, even the two experimental data deviate by a factor of $\sim 1{\cdot}45$.

Table 3. Comparison between experimental and theoretical data for the relative intensities of the resonant $\mathbf{Xe^*(6p_{3/2})\ N_5O_{2,3}O_{2,3}}$ Auger transitions

			$Xe^*\ (6p_{3/2})\ N_5O_{2,3}O_{2,3}$					
Final states		Energy			Rel. intensity			
(a)	(a)	(eV)	(b)	(c)	(d)	(e)	(f)	(g)
$\vert(^3P)6p\ ^2D_{5/2}\rangle$	22	39·73	7·97	7·43	7·91	7·26	5·89	7·37
$\vert(^3P)6p\ ^4D_{7/2}\rangle$	24	39·64	1·58	1·71	1·77	†	3·16	2·05
$\vert(^3P)6p\ ^2S_{1/2}\rangle$	23	39·54	1·76	1·40	0·84	3·31†	1·10	1·09
$\vert(^3P)6p\ ^2P_{3/2}\rangle$	26	39·29	11·35	10·52	19·75	19·36	11·63	19·71
$\vert(^3P)6p\ ^2D_{3/2}\rangle$	31	38·49	9·86	9·51	8·53	8·29	7·14	7·94
$\vert(^3P)6p\ ^4D_{5/2}\rangle$	32	38·47	0·20	0·19	0·003	0·25	0·22	0·31
$\vert(^3P)6p\ ^4D_{1/2}\rangle$	36	38·37	7·47	6·98	3·30	3·78	2·43	3·75
$\vert(^3P)6p\ ^4D_{3/2}\rangle$	34	38·33	1·95	1·81	3·69	4·28‡	2·72	4·27
$\vert(^1D)6p\ ^2F_{7/2}\rangle$	42	37·26	11·29	13·20	3·17	4·70	26·86	13·08
$\vert(^1D)6p\ ^2D_{3/2}\rangle$	43	37·20	12·08	11·93	8·82	7·55	4·78	7·46
$\vert(^1D)6p\ ^2P_{1/2}\rangle$	46	37·07	9·76	8·27	12·83	12·21	8·61	8·59
$\vert(^1D)6p\ ^2D_{5/2}\rangle$	44	37·01	5·69	6·05	9·71	9·87	8·89	8·46
$\vert(^1S)6p\ ^2P_{3/2}\rangle$	67,68	34·52	19·06	20·98	19·53	19·14	16·56	15·92
			Σ100	100	100	100	100	100

(a): The notation of Aksela *et al.* (1995) has been adopted for the states and line numbers.
Present result: (b) no exchange included; (c) exchange included.
Experiment: (d) Aksela *et al.* (1995); (e) Langer *et al.* (1996).
Theory: (f) Aksela *et al.* (1995), FE calculation; (g) Chen (1993).
†Line has not been resolved. ‡Line mix with 5d satellite.

A similar situation occurs for the Auger lines closer to threshold. Here, deviations occur between the different numerical data, between the experimental data, and between theory and experiment, respectively. Thus, the spectrum is fairly well reproduced. At present, none of the theoretical approaches has been able to provide *good* data for *all* of the lines of the resonant Xe $N_5O_{2,3}O_{2,3}$ Auger spectrum. Though, the Auger transitions to the most bound final states

are well reproduced by all theories. This clearly indicates that more advanced studies, using larger basis sets of CSF, are necessary to obtain better numerical data for resonantly excited Auger spectra.

Table 4. Comparison of angular distribution parameters
For an explanation see Table 3

	Xe^* $(6p_{3/2})$ $N_5O_{2,3}O_{2,3}$		
Final states		α_2 par.	
(a)	(a)	(c)	(e)
$\|(^3P)6p\,^2D_{5/2}\rangle$	22	0·704	0·703
$\|(^3P)6p\,^4D_{7/2}\rangle$	24	0·582	0·488†
$\|(^3P)6p\,^2S_{1/2}\rangle$	23	−0·078	†
$\|(^3P)6p\,^2P_{3/2}\rangle$	26	−0·726	−0·919
$\|(^3P)6p\,^2D_{3/2}\rangle$	31	−0·654	−0·516
$\|(^3P)6p\,^4D_{5/2}\rangle$	32	0·214	−0·212
$\|(^3P)6p\,^4D_{1/2}\rangle$	36	−0·750	−0·368
$\|(^3P)6p\,^4D_{3/2}\rangle$	34	0·686	0·099‡
$\|(^1D)6p\,^2F_{7/2}\rangle$	42	−0·109	0·078
$\|(^1D)6p\,^2D_{3/2}\rangle$	43	0·292	0·083
$\|(^1D)6p\,^2P_{1/2}\rangle$	46	−0·291	−1·174
$\|(^1D)6p\,^2D_{5/2}\rangle$	44	0·668	0·460
$\|(^1S)6p\,^2P_{3/2}\rangle$	67,68	−0·550	−0·827

†Line has not been resolved.
‡Line mix with 5d satellite.

(4b) Angular Distribution

The angular distribution parameter α_2 has been recently measured in an experiment by Langer *et al.* (1996). Our numerical results are compared to their data in Table 4. The numbers for transitions with higher Auger energy are well reproduced. In particular, good agreement has been found for the Auger lines 22–24, i.e. transitions to the $(^3\mathrm{P})6\mathrm{p}\,^2\mathrm{D}_{5/2,7/2}$ and $^2\mathrm{S}_{1/2}$ final states.

The transitions to the $(^3\mathrm{P})6\mathrm{p}\,^2\mathrm{P}_{3/2}$ and $^2\mathrm{D}_{3/2}$ states, i.e. lines 26 and 31, show a somewhat larger deviation. For the Auger transition to the $(^3\mathrm{P})6\mathrm{p}\,^2\mathrm{D}_{5/2}$ final state (line 32) we obtain the same magnitude as Langer *et al.* (1996), though our calculation yields the opposite sign. There are discrepancies for transitions which are closer to the ionisation threshold. Note the large anisotropy parameter $\alpha_2 = -1{\cdot}174$ measured by Langer *et al.* for the Auger transition to the $(^1\mathrm{D})6\mathrm{p}\,^2\mathrm{P}_{1/2}$ final state. Though we calculated a negative anisotropy parameter, our calculation underestimates the experimental data by a factor of four.

Thus, the results for the angular distribution parameter confirm the need of large basis sets for a more precise calculation of the Auger emission parameters. The present approach is however sufficient to reproduce the anisotropy parameters for the Auger transitions to the most bound final states.

(4c) Predictions for the Spin Polarisation Vector

Applying the equations of angular distribution and spin polarisation discussed in Sections 2*b* and 2*c* and using the results of Table 2 for the intensities, angular distribution and spin polarisation parameters we are able to give predictions for the spin polarisation vector. We will discuss a few examples in more detail.

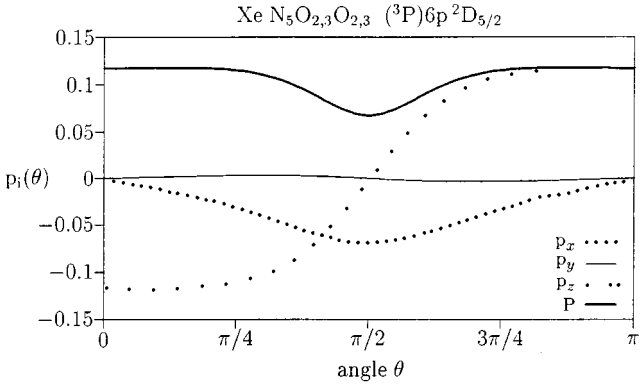

Fig. 4. Cartesian components $p_i(\theta)$, $i = x, y, z$ and magnitude $|P(\theta)|$ of the spin polarisation vector after circularly polarisation synchrotron beam excitation ($|\eta_2| = 1$) as a function of Auger electron emission angle.

First, let us assume a 100% circularly polarisation synchrotron beam, i.e. $|\eta_2| = 1$. Thus, alignment and orientation of the intermediate excited state are given by equation (12) and angular distribution and spin polarisation are given by equations (16)–(19).

As an example, let us consider Auger line 22, i.e. the resonant transition to the $(^3P)6p\,^2D_{5/2}$ final state. Our predictions for the cartesian components of the spin polarisation vector and its magnitude $|P(\theta)|$ are plotted in Fig. 4 against the angle of Auger emission. From our calculation we obtained small values for all spin polarisation parameters. Thus, as shown in Fig. 4, we get only a small overall spin polarisation of less than 13% for this transition. In particular, the dynamic spin polarisation parameter ξ_2 is small (ξ_2 is two magnitudes less than the angular distribution parameter α_2). This results in an almost vanishing component of the spin polarisation vector perpendicular to the reaction plane, $p_y(\theta) \sim 0$.

On the other hand, a large degree of dynamic spin polarisation can be predicted at certain angles for Auger transitions to $J_f = \frac{1}{2}$. We have plotted our results for the components of the spin polarisation vector for the Auger lines 23 and 46, i.e. Auger transitions to the $(^3P)6p\,^2S_{1/2}$ and $(^1D)6p\,^2P_{1/2}$ final states, in Figs 5 and 6.

Concentrating on the component $p_y(\theta)$ of the spin polarisation vector depending on the dynamic spin polarisation parameter ξ_2, we obtain values of $\xi_2 = 0{\cdot}478$ and $\xi_2 = -0{\cdot}404$ for the two transitions which yields a magnitude of more than 40% for the dynamic spin polarisation. Note that the maxima for the dynamic component $p_y(\theta)$ are not at angles 45° and 135°.

Though our calculation yields a slightly larger ξ_2 value for line 23, we suppose line 46, i.e. the $(^1D)6p\,^2P_{1/2}$ final state, to be the best candidate for an experimental determination of a large dynamic component of the spin polarisation vector (see Fig. 6). This is due to the fact that its intensity is approximately six times larger than that of line 23 and covers around 10% of the total intensity of the spectrum.

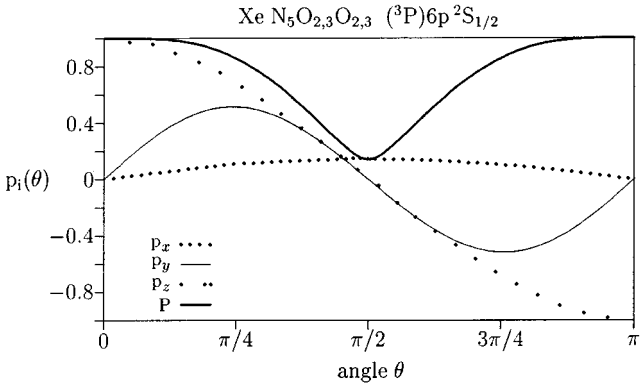

Fig. 5. Cartesian components $p_i(\theta)$, $i = x, y, z$, and magnitude $|P(\theta)|$ of the spin polarisation vector as a function of Auger electron emission angle ($|\eta_2| = 1$, see Fig. 4) for the final state indicated.

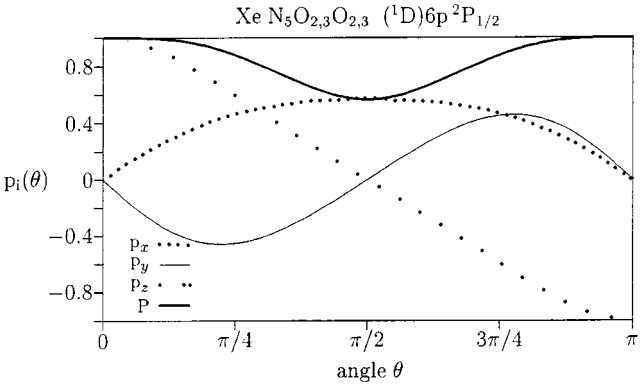

Fig. 6. Cartesian components $p_i(\theta)$, $i = x, y, z$, and magnitude $|P(\theta)|$ of the spin polarisation vector as a function of Auger electron emission angle ($|\eta_2| = 1$, see Fig. 4) for the final state indicated.

(4d) Large Dynamic Spin Polarisation

The discussion in the last section leaves us with the suspicion that Auger transitions to a $J_f = \frac{1}{2}$ final state might have a large dynamic spin polarisation. Our results for these transitions are listed in Table 5 together with theoretical data obtained by Hergenhahn and Becker (1995). From our calculation we obtain the ξ_2 parameter for Auger transitions to $J_f = \frac{1}{2}$ states of the same magnitude or even larger as the angular distribution parameters and the intrinsic spin polarisation parameters ξ_1 and δ_1, respectively. While our results for the transitions to the $(^3P)6p\,^2S_{1/2}$ and $(^1D)6p\,^2P_{1/2}$ final states are of the same order as those obtained by Hergenhahn and Becker, we get a different sign, though still a large ξ_2, for the transition to the $(^3P)6p\,^4D_{1/2}$ state (line 36). Hergenhahn and Becker also obtained a large value of the ξ_2 parameter for the transition to the $(^1D)6p\,^2D_{3/2}$ state (line 43). This is confirmed by our calculation. In conclusion,

though there can be exemptions, from our calculation we obtain large dynamic spin polarisation parameters for all Auger transitions to final states with a total angular momentum $J_f = \frac{1}{2}$. In the following sections we will discuss the physical reasons and explanations for this behaviour.

Table 5. Comparison of dynamic spin polarisation parameter ξ_2
For an explanation see Table 3

	Xe^* $(6p_{3/2})$	$N_5O_{2,3}O_{2,3}$	
(a)	(a)	(c)	(h)
$\vert(^3P)6p\,^2S_{1/2}\rangle$	23	0·478	0·473
$\vert(^3P)6p\,^4D_{1/2}\rangle$	36	−0·164	0·280
$\vert(^1D)6p\,^2D_{3/2}\rangle$	43	0·241	0·247
$\vert(^1D)6p\,^2P_{1/2}\rangle$	46	−0·404	−0·516

Theory: (h) Hergenhahn and Becker (1995).

Reasons. Considering the possibility of interference effects between different partial waves during the Auger emission it is obvious that destructive interference, and thus a small spin polarisation parameter ξ_2, can be expected if a large number of partial waves are emitted. Thus, as a first and necessary propensity rule, we need to restrict the number of partial waves to its minimum, i.e. two,* in order to minimise a decrease of dynamic spin polarisation due to destructive interference.

For photoexcitation of the rare gases we have an intermediate total angular momentum $J = 1$, see e.g. equations (27) and (28). Thus, for Auger transitions to a $J_f = \frac{1}{2}$ state the number of contributing partial waves is reduced to its minimum due to angular momentum coupling rules. As a matter of fact only two partial waves can be emitted for the case considered, i.e.

$$\boldsymbol{J}_f + \boldsymbol{j} = \boldsymbol{J} \longrightarrow j = \tfrac{1}{2}, \tfrac{3}{2}\,, \tag{29}$$

where j denotes the total angular momentum of the Auger partial waves. Thus, destructive interference between the emitted partial waves becomes less likely.

Inspecting the parity of the states we find negative parities π_i and π_f for the intermediate excited and final ionic states, respectively. Note that for photoexcitation of the rare gases the initial state generally has an odd parity. Due to the fact that the Coulomb interaction conserves parity we have

$$\pi_i = \pi_f\,\pi_{\mathrm{Aug}} = \pi_f\,(-1)^{\ell}\,, \tag{30}$$

where π_{Aug} denotes the parity of the emitted Auger partial waves which, in our case, must be even.

Combining equations (29) and (30) we find that only $\varepsilon s_{1/2}$ and $\varepsilon d_{3/2}$ partial waves are emitted. Thus, if the intermediate ionic alignment has been dynamically transformed into the spin polarisation of the Auger electron it will be solely taken away by the $\varepsilon d_{3/2}$ partial wave. Thus, neglecting loss of spin polarisation due to effects like electron-other-electron interaction in the electronic charge cloud during the Auger emission, the transferred dynamic spin polarisation is conserved

* Note that ξ_2 vanishes if only one partial wave is emitted.

in the emitted $\varepsilon d_{3/2}$ partial wave. Even if interference with the $\varepsilon s_{1/2}$ wave takes place it cannot reduce the degree of spin polarisation since the s wave cannot carry away any polarisation at all. Thus, though two partial waves are emitted there can be no decrease in spin polarisation of the emitted Auger electron caused by destructive interference. On the other hand, if $J_f > \frac{1}{2}$, more spin polarisation partial waves with $\pi_{\mathrm{Aug}} = 1$ can be emitted allowing for a destructive interference and thus ξ_2 will decrease.

Table 6. Phase shifts of the partial waves of the Xe^* ($6p_{3/2}$) $N_5O_{2,3}O_{2,3}$ Auger transitions to $J_f = \frac{1}{2}$

For an explanation see Table 3. Data from Lohmann (1998*b*)

Line	$\varepsilon s_{1/2}$		$\varepsilon d_{3/2}$	
no.	σ_c	δ	σ_c	δ
23	0·26940	0·99295	-0·54643	0·44391
36	0·27164	1·02048	-0·55485	0·46739
46	0·27415	1·04328	-0·56467	0·48350

Physical explanation. As an important reason for a large dynamic spin polarisation we consider the phase shift of the partial waves. The total phase σ can be split into the Coulomb phase σ_c and the pure scattering phase δ, i.e.

$$\sigma = \sigma_c + \delta\,. \tag{31}$$

The phase shifts for the Auger lines of the Xe transitions considered are shown in Table 6. From the general expression for ξ_2 (see e.g. Lohmann 1991) it is clear that a large dynamic spin polarisation can only be achieved if the relative phase shift between the two partial waves is $\sim \pi/2$. This is fulfilled for the transitions considered. Our calculation indicates that this is mainly due to the phase shift of the $\varepsilon s_{1/2}$ partial wave caused by its large scattering phase δ which exceeds the pure Coulomb phase by a factor of $\sim 3{\cdot}7$. While for the $\varepsilon s_{1/2}$ partial wave the Coulomb and scattering phase have the same sign, they point in different directions for the $\varepsilon d_{3/2}$ wave. Here, σ_c and δ have approximately the same magnitude and almost cancel each other. Thus, a large spin polarisation parameter ξ_2 is mainly caused by a large phase shift of the $\varepsilon s_{1/2}$ partial wave.

Table 7. Auger energies, relative intensities, anisotropy and dynamic spin polarisation parameters and the spin polarisation at angles θ_m and θ_ξ of our MCDF calculation for the Ar^* ($4s_{1/2}$) $L_3M_{2,3}M_{2,3}$ resonant Auger transitions to final states with $J_f = \frac{1}{2}$ [data are from Lohmann (1998*b*)]

		Ar^* ($4s_{1/2}$) $L_3M_{2,3}M_{2,3}$				
Final states	(eV)	I_0†	α_2	ξ_2	$p_y(\theta_m)$	$p_y(\theta_\xi)$
$\vert(^3P)4s\,^4P_{1/2}\rangle$	213·56	6·889	−1·115	0·0052	−0·0057	−0·0104
$\vert(^3P)4s\,^2P_{1/2}\rangle$	213·07	8·842	0·617	−0·0041	0·0145	0·0082
$\vert(^1S)4s\,^2S_{1/2}\rangle$	208·45	0·114	−0·748	0·0002	−0·0003	0·0004

† Whole multiplet has been normalised to 100.

(4e) Small Dynamic Spin Polarisation

Now, let us discuss the opposite case, i.e. small ξ_2 parameters. For this we consider the example of resonant $\mathrm{Ar}^*(4s_{1/2})L_3M_{2,3}M_{2,3}$ Auger transitions,

$$\gamma + \mathrm{Ar}(^1\mathrm{S}_0) \longrightarrow \mathrm{Ar}^*(2p_{3/2}^{-1}, 4s_{1/2})_{J=1} \searrow \mathrm{Ar}^{+*}(3p^{-2}, 4s_{1/2})_{J_f} + e_A\,. \tag{32}$$

Again, only two partial waves, according to equation (29) are emitted. As pointed out, the parity of the excited intermediate Ar^* state is odd. However, the final ionic state shows an even parity. Thus, from equation (30) we obtain an odd parity $\pi_{\mathrm{Aug}} = -1$ for the Auger partial waves, i.e. the emitted partial waves are $\varepsilon p_{1/2}$ and $\varepsilon p_{3/2}$, respectively. Both p waves may carry parts of the overall spin polarisation. Therefore, it is likely that they show destructive interference which should decrease the spin polarisation for these Auger transitions. Thus, even for transitions to $J_f = \frac{1}{2}$ only a small ξ_2 should be expected. This is confirmed by our calculations of the resonant $\mathrm{Ar}^*(4s_{1/2})\,L_3M_{2,3}M_{2,3}$ multiplet. Our data for the angular distribution and spin polarisation parameters are shown in Table 7. In particular, the dynamic spin polarisation turns out to be approximately two magnitudes smaller than in the Xe case. A full discussion of the photoexcited $\mathrm{Ar}^*(4s_{1/2})\,L_3M_{2,3}M_{2,3}$ Auger spectrum will be published elsewhere.

The Coulomb and scattering phases for the Ar transitions are shown in Table 8. Since the Coulomb phase solely depends on the angular momentum, σ_c has the same value for the $\varepsilon p_{1/2}$ and $\varepsilon p_{3/2}$ partial waves. In contrast to the Xe case, the Coulomb and scattering phases are of the same magnitude but of opposite sign. Thus, we have an almost vanishing phase shift between the two partial waves which eventually yields a small ξ_2. Therefore, we get a small dynamic spin polarisation $p_y(\theta) \sim 0$ for these Auger transitions.

Table 8. Phase shifts of the partial waves of the Ar^* $(4s_{1/2})$ $L_3M_{2,3}M_{2,3}$ Auger transitions to $J_f = \frac{1}{2}$ (data are from Lohmann 1998*b*)

For the identification of states see Table 7

Final state	$\varepsilon p_{1/2}$		$\varepsilon p_{3/2}$	
	σ_c	δ	σ_c	δ
$^4\mathrm{P}_{1/2}$	−0·10779	0·14735	−0·10779	0·13603
$^2\mathrm{P}_{1/2}$	−0·10791	0·14869	−0·10792	0·13737
$^2\mathrm{S}_{1/2}$	−0·10913	0·16172	−0·10913	0·15041

(4f) Propensity Rules

From the above discussion we have been able recently to derive two so-called *propensity rules* (Lohmann 1998*a*) which must be fulfilled for resonant Auger transitions if a large dynamic spin polarisation is to be observed:

- Ensure that only two partial waves are emitted, i.e. preferably investigate Auger transitions of the type

$$J = 1 \longrightarrow J_f = \tfrac{1}{2}\,. \tag{33}$$

This is a necessary but not a sufficient condition and already reduces the number of possible candidates of Auger transitions with a large ξ_2. The second rule is based on parity arguments.

• Ensure that

$$\pi_i = \pi_f \qquad \text{or} \qquad \pi_{\text{Aug}} = 1\,. \tag{34}$$

This prevents destructive interference of spin polarisation between the two partial waves.

The derived propensity rules allow for an easy way of determining whether or not a large dynamic spin polarisation can be expected for a resonant Auger transition. However, one has to keep in mind that these are just propensity rules, i.e. the physics might show a different behaviour for certain Auger transitions. In particular, even for the case of a large number of interfering partial waves, which is the common case for the diagram transitions, there might be the possibility of constructive interference which can in principle bring enhancements of the dynamic spin polarisation. However, besides a few exceptions, these Auger transitions show an almost vanishing dynamic spin polarisation (see e.g. Hahn *et al*. 1985; Merz and Semke 1990; Kabachnik and Sazhina 1988; Lohmann 1993). At present, we are not able to provide any rules or guidelines for the diagram (normal) Auger transitions.

(4g) Predictions for Dynamic Spin Polarisation in Resonant Auger Transitions

Applying the results of the previous discussion we are now able to give predictions for the dynamic spin polarisation in resonant Auger transitions.

A vanishing or small dynamic spin polarisation can be expected e.g. for the following Auger transitions:

$$\mathrm{Ar}^*(4\mathrm{s}_{1/2})\,\mathrm{L}_3\mathrm{M}_{2,3}\mathrm{M}_{2,3} \qquad \mathrm{Kr}^*(5p_{3/2})\,\mathrm{M}_{4,5}\mathrm{N}_1\mathrm{N}_{2,3}$$

$$\mathrm{Xe}^*(6\mathrm{p}_{3/2})\,\mathrm{M}_{4,5}\mathrm{N}_{2,3}\mathrm{N}_{4,5} \qquad \mathrm{Xe}^*(6\mathrm{p}_{3/2})\,\mathrm{N}_{4,5}\mathrm{O}_1\mathrm{O}_{2,3}.$$

For these transitions we predict a small or vanishing dynamic spin polarisation for all transitions of the Auger multiplet.

On the other hand, applying our propensity rules, we predict a large dynamic spin polarisation for resonant Auger transitions to $J_f = \frac{1}{2}$ final states of the following Auger multiplets:

$$\mathrm{Ar}^*(4\mathrm{s}_{1/2})\,\mathrm{L}_3\mathrm{M}_1\mathrm{M}_{2,3} \qquad \mathrm{Kr}^*(5\mathrm{p}_{3/2})\,\mathrm{M}_{4,5}\mathrm{N}_{2,3}\mathrm{N}_{2,3}$$

$$\mathrm{Xe}^*(6\mathrm{p}_{3/2})\,\mathrm{M}_{4,5}\mathrm{N}_{4,5}\mathrm{N}_{4,5} \qquad \mathrm{Xe}^*(6\mathrm{p}_{3/2})\,\mathrm{N}_{4,5}\mathrm{O}_{2,3}\mathrm{O}_{2,3}.$$

(4h) Dynamic Spin Polarisation for Unresolved Fine Structure

Even for an unresolved fine structure of the final state we can predict a non-zero measurable dynamic spin polarisation. Our results for the spin polarisation parameter ξ_2 for the experimentally observed peaks $1b$ and $3b$ of the resonantly excited $\mathrm{Xe}^*(6\mathrm{p}_{3/2})\,\mathrm{N}_5\mathrm{O}_{2,3}\mathrm{O}_{2,3}$ Auger spectrum are shown in Table 9. While our data for the $1b$ peak are in good accordance to theoretical predictions

by Hergehahn and Becker (1995) and by Tulkki *et al.* (1994), we obtain a much smaller average value of the spin polarisation parameter ξ_2 for the peak 3*b*. This can be explained from the fact that the line intensities of lines 43 and 46 are close to each other, and both show a large dynamic spin polarisation, though of opposite sign which eventually results in an almost vanishing averaged dynamic spin polarisation. This can be also seen from the fact that averaging only lines 44 and 46 still results in a large dynamic spin polarisation. Note, that in contrast to the previous tables $\frac{3}{2} \times \xi_2$ is shown.

Table 9. Comparison of the dynamic spin polarisation parameter ξ_2 for averaged final state levels

For an explanation see Table 3

	Xe* ($6p_{3/2}$) $N_5O_{2,3}O_{2,3}$			
Line no.	Peak		ξ_2 par.	
(a)	(a)	(c)	(h)	(i)
22–24	1b	0·089	0·16	0·10
43, 44, 46	3b	−0·008	−0·29	−0·23
44, 46	3b	−0·316		

Theory: (i) Tulkki *et al.* (1994).

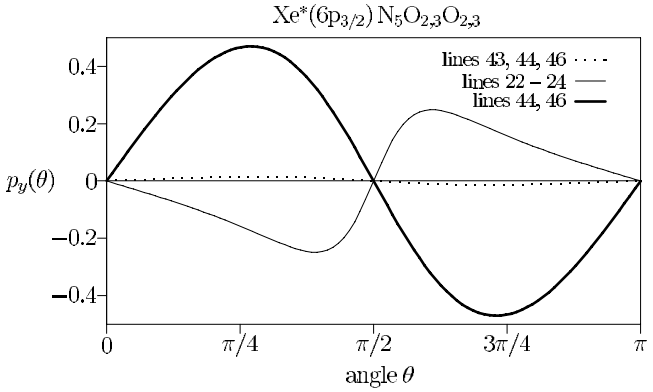

Fig. 7. Dynamic component $p_y(\theta)$ of the spin polarisation vector of the Auger electron as a function of the emission angle for unresolved Auger lines after excitation with a linearly polarisation synchrotron beam ($\eta_3 = 1$).

From the data of Table 9 we are able to give predictions for the spin polarisation vector. Assuming a 100% linearly polarisation ($\eta_3 = 1$) synchrotron beam, only the component $p_y(\theta)$ of the spin polarisation vector, perpendicular to the reaction plane can be non-zero (see the discussion in Section 2*c*). Our results for the dynamic spin polarisation component $p_y(\theta)$ of the unresolved lines 1*b* and 3*b* are plotted in Fig. 7 against the angle of Auger emission. In analogy to the discussion of Section 4*c* we can predict a large degree of dynamic spin polarisation for resonant Auger transitions even for an unresolved fine structure. Degrees of spin polarisation up to more than 40% can be predicted at certain angles. Note that the maximum of the dynamic component $p_y(\theta)$ is not at angles 45° and 135°.

Table 10. Comparison between theoretical and experimental data (Hergenhahn *et al.* 1998) of the dynamic spin polarisation parameter ξ_2 for an unresolved final state level

For an explanation see Table 3 and the text

Line no. (a)	Xe^* $(6p_{3/2})$ $N_5O_{2,3}O_{2,3}$ Peak (a)	ξ_2 par. Theory	Exp.
46, 47	3b	−0·606	−0·61

(4i) Dynamic Spin Polarisation: Comparison with Experiment

Unfortunately, angle and spin resolved experiments are extremely difficult to perform, and thus we are able to compare our predictions to one data set only. Recently, a high resolution experiment has been performed by Hergenhahn *et al.* (1998). Their data are shown in Table 10 in comparison with our theoretical prediction. They observed a large dynamic spin polarisation ξ_2 for the unresolved lines 46–47, where we obtain a large ξ_2 for the sole line 46. Aksela *et al.* (1995) reported the ratio of the relative line intensities as $46/47 = 102/6 \cdot 7$. They identified line 47 as an excited $6p \rightarrow 7s$ shake-up state. Though we have not included shake-up processes in our calculation the ratio of the intensities clearly shows that a large ξ_2 of the unresolved line is mainly caused by a spin polarisation of line 46 which is in good agreement with our prediction.

5. Conclusion

The theory of angle and spin resolved resonant Auger emission has been reviewed by applying a two-step model for the case of a primary photoexcitation. The experimentally accessible quantities, like relative intensities, angular distribution and spin polarisation have been discussed by considering different polarisation states of the incoming exciting photon beam. The relevant parameters of the angle- and spin-resolved spectrum of the resonantly excited $Xe^*(4d_{5/2}^{-1}, 6p_{3/2})_1$ $N_5O_{2,3}O_{2,3}$ Auger transitions have been calculated applying Dirac–Fock methods within a relativistic distorted wave approximation.

The line intensities for the Auger transitions with high energies have been found to be in good agreement with experiment. However, there exist discrepancies between theory and experiment, and between the different theories for transitions with lower energy, i.e. closer to the ionisation threshold. The same behaviour has been be found for the angular distribution parameters. This clearly indicates the need for more advanced calculations, e.g. to include large basis sets of configuration state functions in the calculational approach. From our calculations we predict large spin polarisation parameters for all Auger transitions to final states with a total angular momentum $J_f = \frac{1}{2}$. These results are in good agreement with theoretical predictions by Hergenhahn and Becker (1995) and by Tulkki *et al.* (1994).

Discussing recently derived propensity rules we have presented a method to identify Auger lines for which a large dynamic spin polarisation can be expected. These rules allow for the first time to decide whether an Auger transitions is likely to show a dynamic spin polarisation *before* undertaking the experiment or calculation. We have shown that a large dynamic spin polarisation is caused

by a large scattering phase of the contributing $\varepsilon s_{1/2}$ partial wave, whereas a small spin polarisation is due to a cancellation effect between the Coulomb and scattering phases of the partial waves.

Even for an unresolved final state fine structure we have been able to predict a non-zero measurable spin polarisation provided a $J_f = \frac{1}{2}$ Auger line contributes to the multiplet. This is in good agreement with a very recent experiment by Hergenhahn *et al.* (1999).

Acknowledgments

I am particularly thankful to U. Kleiman for assistance with the numerical calculations. This work has been supported in part by the Deutsche Forschungsgemeinschaft (DFG) with a Habilitation grant and with travel money. The author is thankful to the School of Chemistry of the University of Melbourne where most parts of the manuscript have been prepared. I am particularly grateful to Prof. F. P. Larkins and his group for the hospitality extended to me during my stay. Support by the University of Melbourne with additional travel money is gratefully acknowledged. I am most thankful to Dr U. Hergenhahn of the Fritz-Haber Institut in Berlin and his co-workers who made their experimental data available to me prior to publication.

References

Aksela, H., Sairanen, O. P., Aksela, S., Kivimäki, A., Naves de Brito, A., and Nõmmiste, E. (1995). *Phys. Rev.* A **51**, 1291.
Blum, K. (1996). 'Density Matrix Theory and Applications', 2nd edn (Plenum: New York).
Blum, K., Lohmann, B., and Taute, E. (1986). *J. Phys.* B **19**, 3815.
Chen, M. H. (1993). *Phys. Rev.* A **47**, 3733.
Grant, I. P., McKenzie, B., Norrington, P., Mayers, D., and Pyper, N. (1980). *Comput. Phys. Commun.* **21**, 207.
Hahn, U., Semke, J., Merz, H., and Kessler, J. (1985). *J. Phys.* B **18**, L417.
Hergenhahn, U., and Becker, U. (1995). *J. Elect. Spectrosc. Related Phenom.* **76** 225.
Hergenhahn, U., Kabachnik, N. M., and Lohmann, B. (1991). *J. Phys.* B **24**, 4759.
Hergenhahn, U., Snell, G., Drescher, M., Schmidtke, B., Wiedenhöft, M., Becker, U., and Heinzmann, U. (1999). *Phys. Rev. Lett.*, accepted, and private communication.
Hertel, I. V., and Stoll, W. (1977). *Adv. At. Mol. Phys.* **13**, 113.
Kabachnik, N. M., and Sazhina, I. P. (1988). *J. Phys.* B **21**, 267.
Kabachnik, N. M., Sazhina, I. P., Lee, I. S., and Lee, O. V. (1988). *J. Phys.* B **21**, 3695.
Kabachnik, N. M., Lohmann, B., and Mehlhorn, W. (1991). *J. Phys.* B **24**, 2249.
Kämmerling, B., Krässig, B., and Schmidt, V. (1990). *J. Phys.* B **23**, 4487.
Kessler, J. (1985). 'Polarized Electrons', 2nd edn (Springer: Berlin).
Kessler, J., and Merz, H. (1984). private communication.
Klar, H. (1980). *J. Phys.* B **13**, 4741.
Kleiman, U., Lohmann, B., and Blum, K. (1999). *J. Phys.* B **32**, 309.
Kleinpoppen, H. (1997). private communication.
Kuntze, R., Salzmann, M., Böwering, N., and Heinzmann, U. (1993). *Phys. Rev. Lett.* **70**, 3716.
Langer, B., Berrah, N., and Farhat, A. (1996). *Phys. Rev.* A **53**, R1946.
Lohmann, B. (1991). *J. Phys.* B **24**, 861.
Lohmann, B. (1993). *J. Phys.* B **26**, 1623.
Lohmann, B. (1996). *J. Phys.* B **29**, L521.
Lohmann, B. (1998*a*). *Phys. Rev. Lett.*, submitted.
Lohmann, B. (1998*b*). Habilitation Thesis, University of Münster.
Lohmann, B., and Fritzsche, S. (1994). *J. Phys.* B **27**, 2919.
Lohmann, B., and Fritzsche, S. (1996). *J. Phys.* B **29**, 5711.

Lohmann, B., Hergenhahn, U., and Kabachnik, N. M. (1993). *J. Phys.* B **26**, 3327.
Mehlhorn, W. (1990). *In* 'X-ray and Inner Shell Processes', AIP Conf. Proc. 215 (Eds T. A. Carlson *et al.*), p. 465 (AIP: New York).
Merz, H., and Semke, J. (1990). *In* 'X-ray and Inner Shell Processes', AIP Conf. Proc. 215 (Eds T. A. Carlson *et al.*), p. 719 (AIP: New York).
Müller, N., David, R., Snell, G., Kuntze, R., Drescher, M., Böwering, N., Stoppmanns, P., Yu, S. W., Heinzmann, U., Viefhaus, J., Hergenhahn, U., and Becker, U. (1995). *J. Elect. Spectrosc. Related Phenom.* **72**, 187.
Schmidt, V. (1992). *Rep. Prog. Phys.* **55**, 1483.
Snell, G., Hergenhahn, U., Drescher, M., Schmidtke, B., Müller, N., Wiedenhöft, M., Becker, U., and Heinzmann, U. (1996*a*). BESSY annual report.
Snell, G., Drescher, M., Müller, N., Heinzmann, U., Hergenhahn, U., Viefhaus, J., Heiser, F., Becker, U., and Brookes, N. M. (1996*b*). *Phys. Rev. Lett.* **76**, 3923.
Tulkki, J., Aksela, H., and Kabachnik, N. M. (1994). *Phys. Rev.* A **50**, 2366.

Manuscript received 11 February, accepted 19 April 1999